J Mater Sci (2015) 50:7413–7423
DOI 10.1007/s10853-015-9299-z

Strong reinforcing effects from galactoglucomannan hemicellulose on mechanical behavior of wet cellulose nanofiber gels

Kasinee Prakobna[1,2] · Victor Kisonen[3] · Chunlin Xu[3] · Lars A. Berglund[1,2]

Received: 27 April 2015 / Accepted: 23 July 2015 / Published online: 25 August 2015

Abstract Softwood hemicelluloses could potentially be combined with cellulose and used in packaging materials. In the present study, galactoglucomannan (GGM) is adsorbed to wood cellulose nanofibers (CNF) and filtered and dried or hot-pressed to form nanocomposite films. The CNF/GGM fibril diameters are characterized by AFM, and the colloidal behavior by dynamic light scattering. Mechanical properties are measured in uniaxial tension for wet gels, dried films, and hot-pressed films. The role of GGM is particularly important for the wet gels. The wet gels of CNF/GGM exhibit remarkable improvement in mechanical properties. FE-SEM fractography and moisture sorption studies are carried out to interpret the results for hygromechanical properties. The present study shows that GGM may find use as a molecular scale cellulose binding agent, causing little sacrifice in mechanical properties and improving wet strength.

Electronic supplementary material The online version of this article (doi:10.1007/s10853-015-9299-z) contains supplementary material, which is available to authorized users.

✉ Lars A. Berglund
blund@kth.se

[1] Department of Fiber and Polymer Technology, KTH Royal Institute of Technology, 10044 Stockholm, Sweden

[2] Wallenberg Wood Science Center, KTH Royal Institute of Technology, 10044 Stockholm, Sweden

[3] Johan Gadolin Process Chemistry Center, c/o Laboratory of Wood and Paper Chemistry, Åbo Akademi University, 20500 Turku, Finland

Introduction

The softwood forests in northern Europe are considered as potential sources for a wider variety of bio-based materials from renewable resources. Packaging materials are of particular interest [1, 2]. The challenge is to combine biodegradability with competitive mechanical performance as compared with synthetic polymers used in packaging films, containers, and boxes. Wood-based materials are available in large quantities, and there is an existing industrial infrastructure, which can handle rapid increases in demand. The present study deals with the potential application of softwood hemicelluloses as polymer matrix materials for composites.

The wood cell wall consists of a hydrated polymer network, which is composed predominantly of polysaccharides. The polysaccharide structures, in particular cellulose, provide essential mechanical functions to the cell wall [3]. The fibrous network or lamellae of cellulose microfibrils serves as the principal scaffold, whereas the hemicellulose matrix separates microfibrils and provides ductility by forming a hydrated matrix yet able to transfer stress. In the secondary cell wall of Norway spruce (*Picea Abies*), a framework of cellulose microfibrils is primarily associated with *O*-acetyl galactoglucomannan (GGM) [4], which is the most abundant hemicellulose.

Cellulose is a linear β-1,4-D-glucan chain that assembles into cellulose microfibrils. The repeating unit of cellulose is illustrated in Fig. 1, for the purpose of comparison with GGM. Cellulose molecules arrange themselves in fully extended chain conformation with crystalline and short non-crystalline regions [5], and form cellulose microfibrils with a diameter of 3–4 nm [6]. The crystalline structure of cellulose microfibrils is associated with unique mechanical properties such as high modulus of the cellulose I crystal

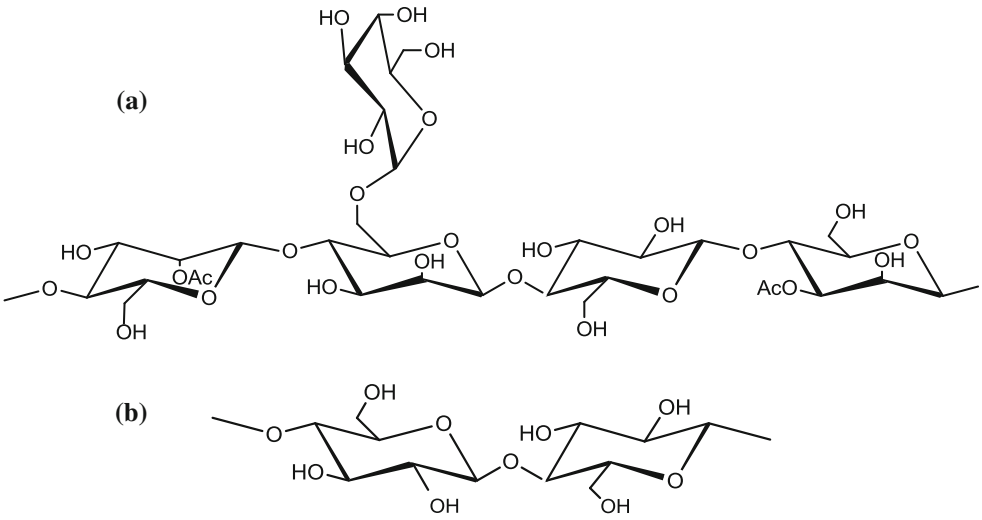

Fig. 1 Chemical structure of **a** galactoglucomannan (GGM) and **b** cellulose

(130–150 GPa) [7–9] and high strength of disintegrated cellulose nanofibers (CNF) (1.6–3.0 GPa) [10]. These intrinsic mechanical properties are promising for high-performance biocomposite materials. Nanoscale fibrous cellulose can be extracted from chemical wood pulp in the form of CNF. To reduce energy requirements, the CNF preparation can be performed via enzymatic pretreatment [11] or chemical oxidation pretreatment [12], combined with mechanical disintegration [13]. The obtained CNF is stable and available as a water suspension. Therefore, it can be readily used as a reinforcement for water-soluble polymers such as hemicelluloses [14–17].

GGM is the principal structural cell wall hemicellulose in Norway spruce (approximately 20 wt% of the dry wood tissue) [18]. The backbone of GGM is a linear β-1,4-D-mannopyranosyl randomly linked with β-1,4-D-glucopyranosyl units. Acetyl substituents (Ac) are attached to either C-2 or C-3 positions of mannose, and this is significant. Some fraction of the mannose residues are substituted by α-1,6-D-galactopyranosyl units (Fig. 1). The ratio of mannose:glucose:galactose can vary in the range of 3.5–4.5:1:0.5–1 for Norway spruce GGM [18–20]. GGM can be isolated in a large scale by ultrafiltration of the process water resulting from thermomechanical pulping [20]. It can also be extracted from softwood by pressurized hot water extraction [21]. GGM-based films could potentially be used in packaging due to good barrier properties for oxygen diffusion [21, 22]. However, the mechanical properties of GGM are insufficient. Low molar mass and hydrophilic characteristics result in poor mechanical properties, moisture sensitivity, and poor film forming properties. One approach to address these limitations of GGM is to use CNF reinforcement [15]. The addition of CNF leads to increased modulus, and tensile strength of the nanocomposite film. The moisture sorption of the film is also reduced. This makes it more suitable for packaging applications [2]. Even though film forming properties can be improved by plasticizers [22, 23], moisture sensitivity is increased [21].

In recent years, "bioinspired or biomimetic nanocomposites" based on wood CNF [16, 24–27] have been investigated; where the nanostructure and physical properties of plant cell walls provide inspiration. In this approach, the nanofibrillar network of CNF is the main load-bearing component, which results in biocomposite materials with high modulus and strength [28]. Moreover, a soft polymer matrix can result in improved ductility and toughness [25, 29, 30], analogous to the function of hemicelluloses [31–33] in the plant cell wall. The mechanical properties of the CNF-based biocomposites can be further developed with better control of polymer matrix distribution at nanoscale [17, 27]. The individual CNF nanofibers are coated by a uniform layer of adsorbed polysaccharide matrix. This makes it possible to do filtration without loss of polymer matrix. This is analogous to the distribution of hemicelluloses in the plant cell wall, where they adsorb to cellulose microfibrils during plant cell wall biosynthesis. Strong effect of matrix distribution has been demonstrated for hygromechanical properties of the biocomposites [17, 27]. However, the mechanical properties of composite films based on GGM-coated CNF [16] were lower than expected.

The effect of GGM addition to CNF nanofibers and corresponding CNF/GGM nanopaper films is investigated in the present study. The objective is to assess the material structures and properties and learn about the role of GGM as it is present in the form of a CNF coating. Three different forms of nanocomposites are prepared by filtration including wet gels, "solid films," and hot-pressed films.

Experimental section

Material components

CNF were extracted from never-dried spruce sulfite pulp (Nordic Paper Seffle AB, Sweden) by enzymatic pretreatment and mechanical disintegration, according to previously developed method [11, 28]. In brief, the pulp was treated with endoglucanase enzyme (Novozyme 476, Denmark) to facilitate mechanical fibrillation. The pretreated pulp was subsequently subjected to disintegration using a microfluidizer (Microfluidics Ind., USA). The CNF was obtained after passing 3 times through big chambers (400 and 200 μm) and 5 times through small chambers (200 and 100 μm). A CNF suspension with a concentration of 2 wt% was successfully prepared. The resulting CNF contains 14.0 wt% total hemicelluloses, consisting of 8.0 wt% native GGM derived from raw material.

GGM was isolated from process water of thermomechanical pulping as was previously reported [34, 35]. Shortly, the process water containing GGM was concentrated and purified using different filtration and ultrafiltration techniques. The GGM concentrate liquor was subjected to ethanol precipitation (70 %, three times) for further purification. The ethanol-precipitated GGM-cake was dried in a vacuum desiccator at 40 °C. The resultant GGM has an average molar mass of 39 kg/mol determined in 0.1 M $NaNO_3$ eluent by size exclusion chromatography in online combination with a multi-angle laser-light-scattering at three scattering angles of 41.5°, 90.0°, and 138.5° ($\lambda_0 = 690$ nm, miniDAWN, Wyatt Technology, Santa Barbara, USA) and with a refractive index detector (Shimazu Corporation, Japan). A two column system 2× Ultrahydrogel TM linear 7.8 × 300 mm and a guard column were used. The samples were filtered through a 0.22-μm nylon syringe filter before the injection. The d_n/d_c value of 0.15 was used [36]. Data processing was performed with Astra software (Wyatt Technology, Santa Barbara, USA). The complete sugar composition of GGM was analyzed by gas chromatography after an acid methanolysis and silylation as previously reported [37].

For preparation of nanocomposite materials, the GGM powder was dispersed in deionized water to a final concentration of 0.1 wt%. The solubility of the GGM solution was improved by heating at 90 °C.

Preparation of CNF and CNF/GGM nanocomposites

CNF and CNF/GGM nanocomposites were prepared from a suspension of CNF (2 wt%) and GGM (0.1 wt%). For the CNF nanocomposite, the CNF suspension was diluted to 0.2 wt% in deionized (DI) water and subjected to high-shear mixing using an Ultra Turrax mixer (Ika, T25 Digital) at a speed of 8000 rpm for 3 min. In the case of CNF/GGM nanocomposites, aqueous suspensions of CNF/GGM mixture with varying GGM contents [10, 20, 40, 50, 67 wt% with respect to total dry mass (CNF + GGM)] were prepared. They were mixed thoroughly at 90 °C for 4 h using magnetic stirring. The obtained CNF/GGM mixtures were then diluted to 0.2 wt%, based on CNF dry weight, in DI water. High-shear mixing was further applied to CNF/GGM suspensions, as described above for CNF. Prior to film/network formation, the diluted CNF and CNF/GGM suspensions were subjected to degassing in a vacuum chamber for 10 min. The CNF and CNF/GGM nanocomposites were prepared in three different forms:

i. Wet gels—free-standing wet gels of CNF and CNF/GGM were prepared from the diluted CNF and CNF/GGM suspensions. The suspensions were vacuum filtered on a glass filter funnel with a filter membrane (0.65 μm, DVPP, Millipore), according to the method reported previously [28]. After filtration, free-standing wet gels were formed on top of the membrane. The solid content of wet gels, determined by drying samples at 105 °C overnight to reach steady state condition, was in the range of 15–18 wt%.
ii. Solid films—to obtain solid films, the wet gels of CNF and CNF/GGM nanocomposites were simply dried using a laboratory sheet dryer (Rapid Köthen), as described by Sehaqui et al. [38]. They were placed between two porous metal wire membranes, and subjected to drying for 10 min. The obtained materials were designated as "solid films," containing—7 wt% moisture in a conditioned room at 23 °C and 50 RH %.
iii. Hot-pressed films—hot-pressing was performed on the obtained CNF and CNF/GGM solid films, containing 6–7 wt% moisture. The samples were placed between hot metal plates, and heated at 120 °C under pressure of 5 MPa for 15 min.

Since a substantial amount of GGM was lost during filtration, the remaining GGM content in the nanocomposites was determined by sugar analysis. To prepare solubilized monosaccharides for the analysis, all samples were subjected to freeze-drying and then acid hydrolysis according to a standard method SCAN-CM 71:09. The obtained solutions were quantified using high-performance anion exchange chromatography with pulsed amperometric detector (HPAEC-PAD) equipped with a Dionex ICS-300 system (Dionex, Sunnyvale, USA). The remaining content of GGM after film preparation is reported in Fig. 2. CNF/GGM nanocomposites of three different GGM contents were selected for further experiment. It is noted that the neat CNF contains 8.0 wt% of native GGM derived from spruce wood pulp. Total GGM content, including native GGM and remaining GGM content in the CNF, is shown in Table 1.

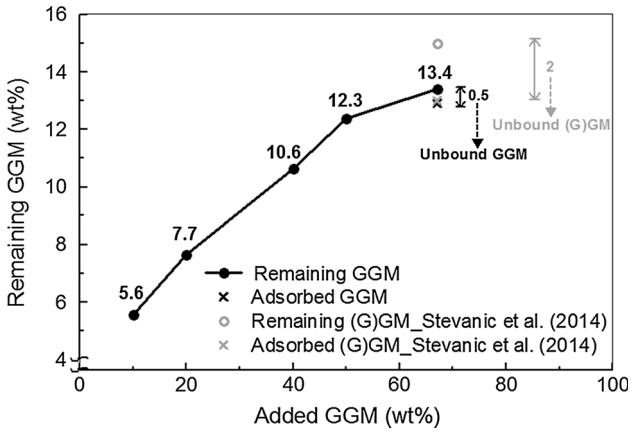

Fig. 2 Remaining amount of GGM on the CNF/GGM nanocomposite. Results include data from Stevanic et al. [16] where partially debranched galactoglucomannan, i.e., spruce (galacto)glucomannan, (G)GM, was investigated

Table 1 Weight percentage of GGM in raw material (Spruce pulp fiber), GGM fraction after film preparation, and total GGM content in the final materials

Sample	Native GGM (%)[a]	GGM from film preparation (%)	Total GGM (%)
Spruce pulp fiber	8.0	–	8.0
CNF/GGM 5.6 wt%	8.0	5.6	13.6
CNF/GGM 10.6 wt%	8.0	10.6	18.6
CNF/GGM 13.4 wt%	8.0	13.4	21.4

[a] Note that native GGM content from raw material was analyzed by acid methanolysis

Dynamic light scattering (DLS)

Qualitative determination of hydrodynamic measures in CNF suspensions was carried out using a Zetasizer Nano ZEN3600 (Malvern Instruments Ltd., UK). Prior to DLS measurement, the aqueous suspensions of CNF were diluted to a final concentration of 100 mg/L, and then filtered through 5-μm membrane (Acrodisc) to avoid interference from impurities. The DLS measurements were performed at 25 °C. The reported data for size distribution of nanofibers were averaged from several measurements.

Atomic force microscopy (AFM)

AFM height images of nanofibers for CNF and CNF/GGM nanocomposites were collected using tapping mode of Nanoscope IIIa AFM (Veeco Ltd, USA). The diluted suspensions of nanofibers were spin-coated and dried on mica disks (Ted Pella Inc, USA). Silicon cantilevers (Bruker, UK) having a nominal tip radius of 8 nm and a spring constant of 5 N/m were used. AFM images with a scanned area of 2×2 μm^2 were collected. The height profile from AFM images represents nanofiber diameter. The distribution of nanofiber diameters was recorded based on at least 300 height profiles of each sample.

Field-emission scanning electron microscope (FE-SEM)

FE-SEM images showing nanofibrillar network and fracture surfaces obtained from CNF and CNF/GGM nanocomposite were taken with a Hitachi S-4800 FE-SEM. To observe the nanofibrillar network, it is crucial to limit the nanofiber aggregation during water evaporation. Hence, the samples were subjected to supercritical drying under liquid CO_2 (SC-CO_2) using a critical point dryer (Autosamdri-815, Tousimis, USA) [39]. High porosity nanofibrillar network ($\approx$80 %porosity) was obtained. The difference of nanofibrillar network with and without GGM was compared in order to observe the role of GGM in the nanocomposite. To observe the microstructure of nanocomposites, fracture surfaces of solid films and hot-pressed films for CNF and CNF/GGM were observed after tensile testing. To avoid charging during FE-SEM observation, all samples were sputtered with an ultra-thin layer of graphite and gold–palladium using Agar HR sputter coater.

Tensile testing

Tensile properties of CNF and CNF/GGM nanocomposites were measured using Instron 5944 instrument equipped with a 500 N load cell. The samples were cut into a rectangular strip with a dimension of 5×30 mm^2. Prior to tensile testing, the solid films and hot-pressed films were conditioned at two different relative humidities of 50 and 85 RH % for a week. Tensile testing was conducted in a conditioned room at 23 °C and 50 RH %. The testing was performed at a strain rate of 10 %/min and an initial grip distance of 20 mm. Tensile properties were presented as average values from 5 to 8 measurements.

In addition, digital speckle photography (DSP) measurement was carried out to correct the grip displacement and obtain accurate strain data. Strain values were analyzed using Vic 2D software. Accurate values of Young's modulus were correlated from the DSP calibration.

Dynamic vapor sorption (DVA)

Moisture sorption behavior of solid films and hot-pressed films for CNF and CNF/GGM nanocomposites was investigated using a DVS instrument (Surface Measurement Systems Limited, UK). Prior DVS measurement, the samples were dried in a vacuum oven at 40 °C overnight. The samples were then dried in the DVS cell. The relative humidities (RH %)

were consecutively increased from 0 to 20, 40, 60, 80, and 90 RH %. The sample was weighed in different humidity atmosphere when the equilibrium was reached, and the moisture sorption was calculated according to the following equation:

$$\text{Moisture uptake} = 100 \times \frac{W_{\text{moist}} - W_{\text{dry}}}{W_{\text{dry}}},$$

where W_{moist} is the sample weight equilibrated at certain RH % and W_{dry} is the dry weight of the sample at 0 RH %. The reported data were based on duplicate measurements.

Results and discussion

Preparation of CNF/GGM nanocomposite

A CNF/GGM nanocomposite was prepared by filtration of an aqueous mixture of CNF and GGM. CNF is expected to form a porous network structure with GGM replacing the pore space. Various GGM contents were used in the suspensions. The residual GGM content in CNF/GGM after filtration was determined, and the result is presented in Fig. 2. GGM content increased from 5.6 to 13.4 wt% when GGM addition to the suspension was varied from 10 to 67 wt%. The CNF/GGM nanocomposite with a GGM content of 13.4 wt% consists of 0.5 wt% unbound GGM and 12.9 wt% adsorbed GGM, showing that the large majority of residual GGM is adsorbed onto CNF. Filtration times were unchanged between neat CNF and core–shell CNF/GGM. This indicates that GGM has little effect on water holding capacity of CNF. The observed degree of sorption is in agreement with previous data [16] where CNF and debranched—GGM—were studied. Mannans with low extent of side chain substitution are still expected to show interaction with cellulose at the molecular level [40]. Figure 2 compares the remaining and unbound content of GGM versus (G)GM in the nanocomposites between two studies. The water solubility of (G)GM, the less substituted molecule, is expected to be lower than for GGM [16]. The slightly higher amount of (G)GM in the nanocomposite is probably due to increased unbound (G)GM content. It is noted that the amount of adsorbed GGM is low (less than 50 %) compared to results for xyloglucan [17], another hemicellulose. This is in accordance with a sorption study using QCM-D, showing that the chemical structure of hemicelluloses has strong effects on adsorption to cellulose [41]. The difference in adsorbed amount also depends on molar mass [42].

DLS data of CNF and CNF/GGM nanofibers in mixed suspension

Since the nanocomposite network is formed during filtration of CNF and CNF/GGM suspensions, their dispersion state influences final structure and properties of the materials. Figure 3 displays the hydrodynamic size distributions of nanofibers from CNF and CNF/GGM with various GGM contents (5.6 and 10.6 wt%). Bimodal and very similar distributions were observed for neat CNF and CNF/GGM 10.6 wt%. The peak at larger size (400 nm) is expected to arise from large-sized aggregates, which may be present in small fraction. For CNF/GGM 5.6 wt%, a unimodal distribution with a more narrow peak at 265 nm is observed. The extent of aggregation for CNF/GGM 5.6 wt% is expected to be lower than for CNF and CNF/GGM 10.6 wt%. Hence, the CNF/GGM 5.6 wt% may be a promising condition for preparation of well-dispersed nanocomposite. A similar although more apparent effect was reported for CNF with xyloglucan [17]. Due to the expected affinity of GGM to cellulose [43], GGM molecules adsorbed to the CNF surface and influenced the dispersion of CNF in suspension [44, 45].

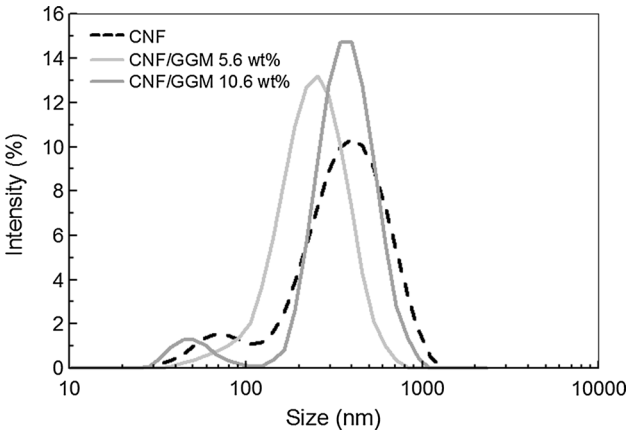

Fig. 3 Estimated hydrodynamic size distributions of CNF and CNF/GGM in aqueous suspensions, based on dynamic light scattering (DLS) data. Note that the reported data are based on an assumption of spherically shaped particles

Nanostructure of CNF and CNF/GGM nanofibers

The distributions of nanofiber diameter for CNF and CNF/GGM containing 10.6 wt% GGM are presented in Fig. 4a, b, respectively. In Fig. 4a, it is observed that the diameter of CNF is typically less than 10 nm (95 % of the population). The majority are in the range of 3–6 nm, which is close to the diameter of cellulose microfibrils in spruce wood [46]. The nanofibers with larger diameters are nanofiber aggregates. For CNF/GGM 10.6 wt% (Fig. 4b), the average diameter is slightly larger, but the number of nanofibers with diameter below 10 nm is still substantial, corresponding to 90 % of the population. The fraction of small nanofibers in the range of 3–6 nm is reduced compared to neat CNF. Statistical analysis yields a number

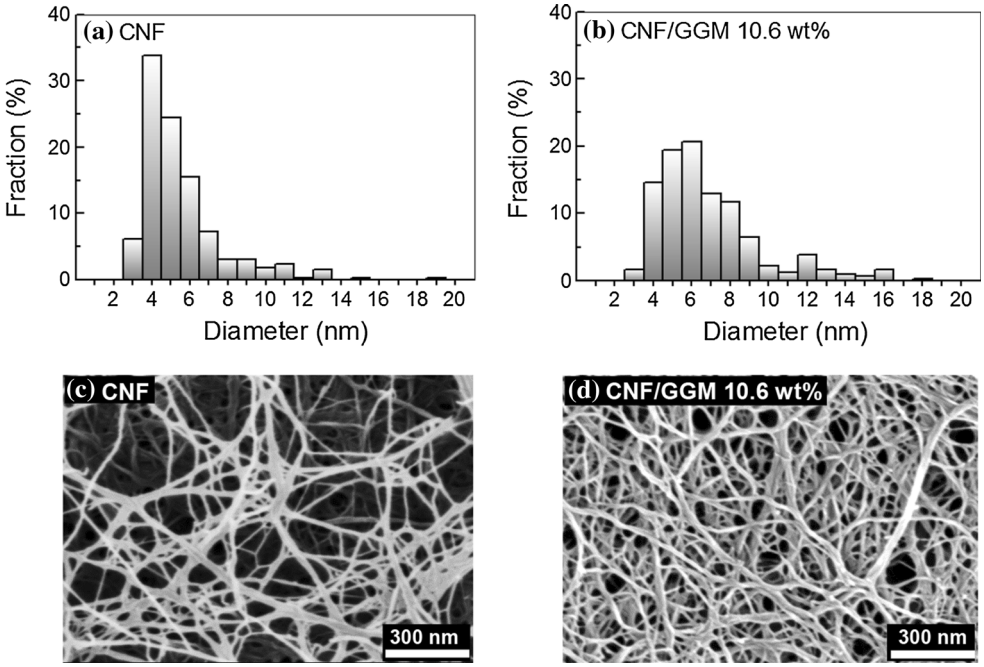

Fig. 4 Height distributions of **a** CNF nanofibers and **b** CNF/GGM nanofibers containing 10.6 wt% GGM measured on AFM images. Lower micrographs are FE-SEM images of their nanofibrillar networks based on **c** neat CNF and **d** CNF/GGM 10.6 wt% prepared under supercritical CO_2 drying

Fig. 5 Schematic illustration of nanofibrillar network in CNF/GGM nanocomposite. Note that the solid materials will have very low porosity

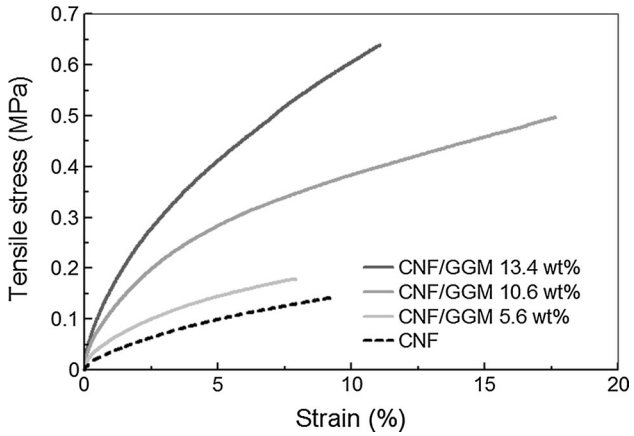

Fig. 6 Tensile stress–strain curves for wet gels prepared from neat CNF and CNF/GGM nanocomposites, with different GGM contents. The solid content is in the range of 15–18 wt%, see Table 2

average and weight average diameter (d_n and d_w) of 4.7 and 5.9 nm for CNF, which is substantially increased to 6.1 and 7.7 nm for CNF/GGM 10.6 wt%. The nanofibrillar networks are very different for CNF and CNF/GGM 10.6 wt% as appeared in Fig. 4c, d. In order to limit aggregation of nanofibers during drying, the materials were prepared under supercritical CO_2 drying. Thin strands are less prominent in the case of CNF/GGM 10.6 wt%. Moreover, it appears that CNF/GGM nanofibers can self-assemble into larger bundles. This indicates that GGM on the surface of CNF plays a role in binding adjacent nanofibers and forms networks. Based on the average molar mass of GGM (39 kDa), the theoretical chain length of GGM molecules is approximately 100 nm. One may speculate that the GGM molecules adsorb to CNF, and the chain length is sufficient to provide physical crosslinking [47] between adjacent nanofibers. Based on the result obtained from AFM analysis and FE-SEM observations, a structure for the nanofibrillar network in the CNF/GGM nanocomposite is proposed in Fig. 5.

Wet gels based on CNF and CNF/GGM

The stress–strain behavior in tension of wet gels from CNF and CNF/GGM is presented in Fig. 6, and the corresponding data are presented in Table 2. All wet gels have comparable solid content in the range of 15–18 %. The association of GGM in the CNF/GGM network has a positive influence on

Table 2 Tensile properties for wet gels prepared from CNF and CNF/GGM nanocomposites

Wet gels	Solid content (%)	Young's modulus (MPa)	Tensile strength (MPa)	Elongation (%)	Work of fracture (kJ/m^3)
CNF	14.9	4.1 (0.5)	0.11 (0.04)	9.2 (2.1)	8.2 (3.0)
CNF/GGM 5.6 wt%	15.1	5.9 (2.2)	0.15 (0.03)	8.3 (1.0)	7.8 (1.7)
CNF/GGM 10.6 wt%	18.0	21.3 (2.0)	0.33 (0.04)	15.8 (3.0)	46.0 (10.1)
CNF/GGM 13.4 wt%	16.9	28.8 (6.6)	0.65 (0.16)	10.9 (1.3)	50.8 (12.8)

The results are averages of at least five specimens with their standard deviation

the properties of wet gels and this must be related to physical GGM crosslinking of CNF, analogous to the plant cell wall. Due to the presence of hydroxyl groups on adsorbed GGM, this hemicellulose may act as a bonding agent, increasing CNF–CNF interaction through hydrogen bonding. As the GGM content increases, the Young's modulus and tensile strength are increased. Moreover, the elongation (strain to failure) and work of fracture are improved at high GGM content (10.6 and 13.4 wt%). The CNF/GGM 13.4 wt% exhibits modulus, strength, and work of fracture roughly 6–7 times higher than for CNF.

The results point strongly in the direction of a CNF–GGM network, where GGM segments are adsorbed to CNF but also form physical links in the form of molecular tethers between individual CNF. These physical links are apparently very important in wet gels. They serve to increase gel stiffness through crosslink action, so that stress is increased for a given strain. The estimated 100 nm length of individual GGM molecules is apparently sufficient to serve the crosslinking function. Without added GGM, the interaction between CNF is weakened and the wet gel fails at lower strain and stress. In addition to the effect of physical crosslinking, strong interfacial adhesion between cellulose and hemicelluloses could also be another explanation for remarkably improved tensile properties in the wet gels of CNF/GGM.

Solid films and hot-pressed films of CNF and CNF/GGM

Fracture surfaces were investigated using FE-SEM (Fig. 7a, b). Both "solid film" and hot-pressed film exhibited a layered structure [28]. The appearance of lamellar structure is more noticeable in the CNF solid film (Fig. 7a). Possibly, the interlayer bonding is weaker without hot-pressing. The solid film has a more jagged and rough appearance with nanofibers protruding from the fracture plane. In the CNF hot-pressed film (Fig. 7b), the fracture surface was more smooth with less CNF pull-out. In CNF hot-pressed film, the interlayer, and possibly interfiber bonding, is stronger since CNF–CNF fusion aided by GGM takes place during hot-pressing [48].

The solid films in Fig. 8 are prepared by drying and appear differently than hot-pressed films. The lamellar structure is more apparent, in particular for the neat CNF composition in Fig. 8a. Increasing GGM content appears to better bind lamellae together, see Fig. 8b, c. Fractured CNF nanofibers are apparent on fracture surfaces although lamellae appear to fail as individual layers.

The hot-pressed materials have a more smooth fracture surface with less delamination, see 8d,e,f. Smoothness increases with GGM content. There are signs of nanofiber bundle aggregates [49] at the scale of 20–40 nm, and the GGM phase has been deformed plastically as CNF layers are delaminated (peeled apart). In Fig. 8c–f, there is a sign of GGM-rich regions in CNF/GGM 13.4 wt%. Perhaps GGM molecules could migrate within the nanofibrillar network during drying process. It is reported in the literature [15] that the glass transition temperature (T_g) of spruce GGM is in the vicinity of temperature applied for drying at 93 °C.

The mechanical behavior in uniaxial tension of CNF/GGM solid films and hot-pressed films conditioned at 50 and 85 RH % is presented in Fig. 9, and associated properties are given in supporting information (Table S1 and S2). In general, the stress–strain behavior is very similar for CNF and CNF/GGM solid films, and the effect of increasing GGM content is weak in this composition range.

At 50 RH % (Fig. 9a, c), the main effect of hot-pressing is to increase yield strength and decrease strain to failure. This is consistent with improved interlaminar and CNF/GGM adhesion and possibly reduced porosity. As the relative humidity is increased, the mechanical properties are somewhat decreased although hot-pressing has strongly favorable effects. Again, this is consistent with decreased porosity and/or improved interlaminar and CNF/GGM adhesion. Young's modulus of CNF and CNF/GGM solid films is in the same range of 13.5–13.8 GPa at 50 % RH. The knee in the stress–strain curves is followed by strong strain-hardening due to reorganization of the nanofibrillar network [28]. Tensile failure of CNF/GGM solid films occurred at lower strain compared to CNF. Strong interfacial adhesion between cellulose and GGM could be the explanation [40, 50]. It is possible that the slippage of nanofibers is restricted due to strong CNF–GGM adhesion,

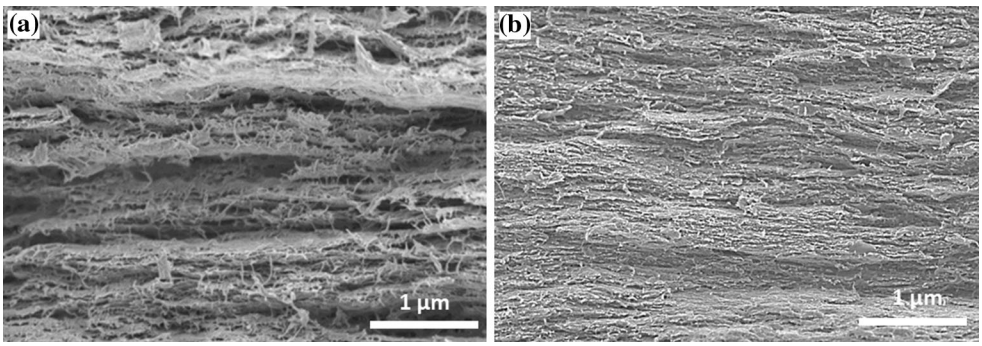

Fig. 7 FE-SEM images of tensile fracture surfaces for **a** CNF solid film and **b** CNF hot-pressed film

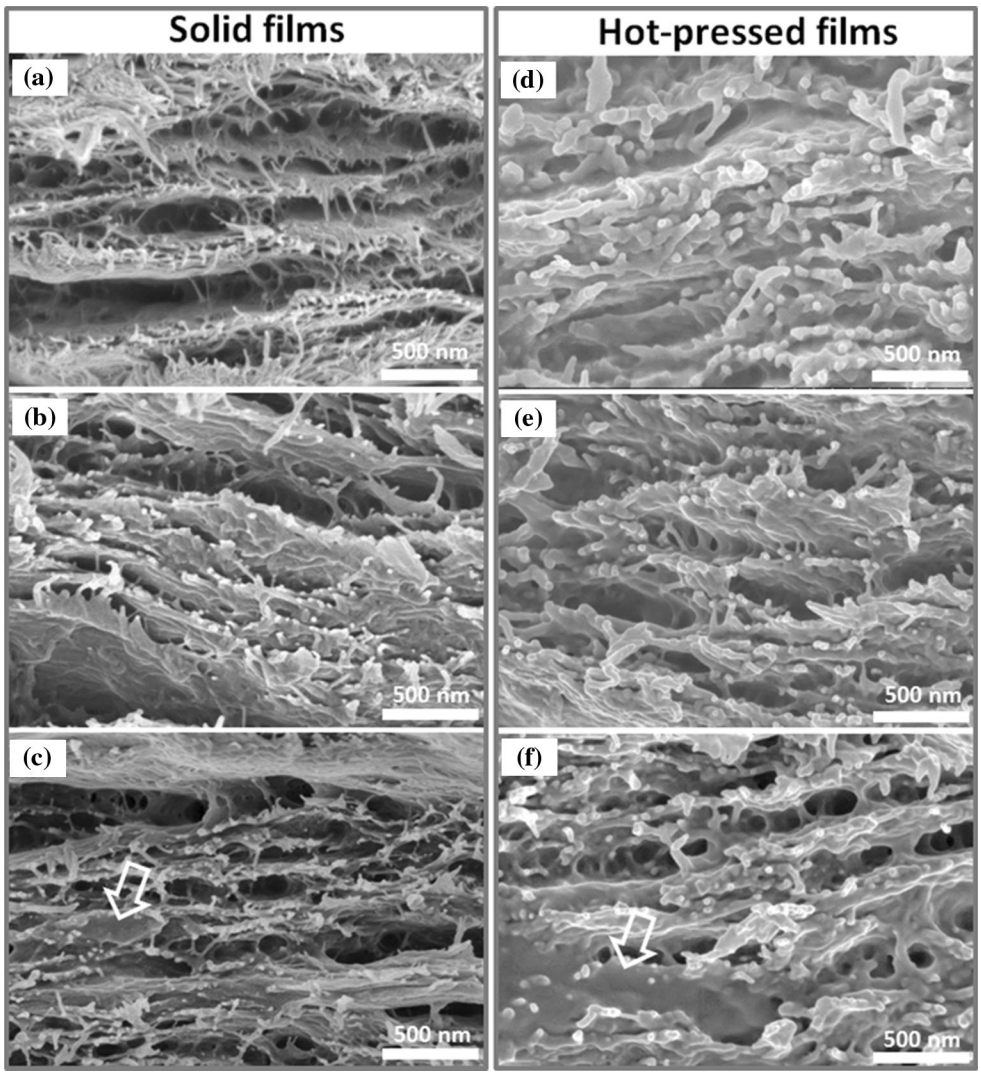

Fig. 8 FE-SEM images at high magnification of tensile fracture surfaces for solid films of **a** CNF, **b** CNF/GGM 5.6 wt%, **c** CNF/GGM 13.4 wt% and hot-pressed film of **d** CNF, **e** CNF/GGM 5.6 wt%, **f** CNF/GGM 13.4 wt%. The arrow indicates GGM-rich region in the CNF/GGM 13.4 wt% film

leading to film embrittlement [51] at 50 % RH. Pores may be able to facilitate nanofiber slippage for CNF solid films.

Compared with an earlier study of CNF/(G)GM [16], the present data are higher, see Table S1. Since the neat CNF nanopaper data are also higher, it is likely that the distribution of CNF is more favorable. Reasons may include fewer CNF aggregates, lower porosity, or better in-plane CNF orientation distribution.

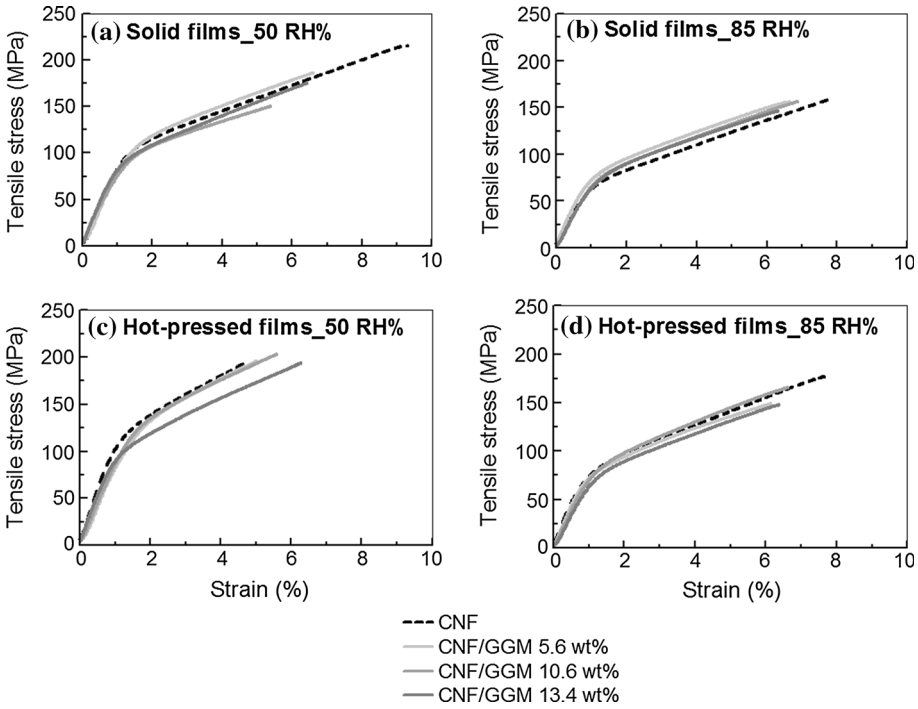

Fig. 9 Tensile stress–strain curves for solid films and hot-pressed films prepared from CNF and CNF/GGM nanocomposites. The samples were conditioned at two different relative humidities (50 and 85 RH %)

Moisture sorption for solid films and hot-pressed films of CNF and CNF/GGM nanocomposites

Moisture sorption curves of CNF, GGM, and CNF/GGM are presented in Fig. 10a, b. The curves had a sigmoidal shape which is a characteristic of sorption isotherm type II [52]. As expected, the moisture sorption data of neat CNF and CNF/GGM films were much lower than that of neat GGM, reflecting more abundant moisture sorption sites in amorphous polymers [53]. Interestingly, the solid film of CNF/GGM 5.6 wt% had slightly lower moisture sorption than that of neat CNF nanopaper, while hot-pressed films showed identical moisture sorption behavior. Good interfacial adhesion [54] between CNF–GGM is expected, and GGM molecules may have different conformations compared with in neat GGM films. For CNF/GGM 13.4 wt% films, the moisture sorption was slightly increased, which might be influenced by local GGM-rich matrix regions apparent in FE-SEM images (Fig. 8c, f). The result observed for CNF/GGM 13.4 wt% is similar to an earlier study of CNF/(G)GM film reported by Stevanic et al. [16]. Hot-pressing effects have not been studied before, and those films showed less moisture sorption than "solid films" throughout the observed RH % (Fig. 10b).

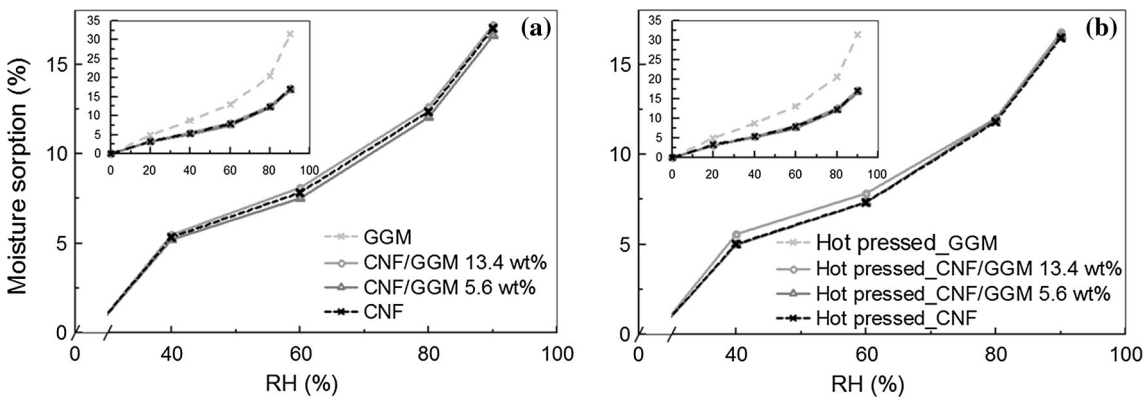

Fig. 10 Moisture sorption isotherms for **a** solid films and **b** hot-pressed films prepared from CNF and CNF/GGM nanocomposites. The data are average values from two measurements, and the symbols are representative of experimental error. The dynamic vapor sorption (DVS) results are compared with moisture sorption of neat GGM presented in the inset

Conclusions

GGM is a unique hemicellulose for softwoods and is abundant in Norway spruce (Picea Abies). We have designed wood-based films based on core–shell nanofibers from CNF and GGM. Only small amounts of GGM adsorb to CNF for the present preparation conditions. Compared with neat CNF, CNF/GGM wet gels exhibited outstanding mechanical properties combining modulus, strength, and toughness. Although only 13 % GGM was added, modulus and strength increased 6–7 times compared with CNF at similar solids content. This dramatic improvement is attributed to GGM acting as physical crosslinks between CNF fibrils so that the "crosslink density" increases and is preserved during mechanical deformation. The present nanocomposite is thus successfully mimicking the roles of cellulose microfibrils and GGM in the plant cell wall.

The CNF/GGM fibrils with adsorbed GGM show increased average diameter ($d_n = 6.1$ nm compared with $d_n = 4.7$ nm), consistent with an adsorbed GGM "shell" layer. In general, stress–strain curves of the CNF/GGM are similar to those from neat CNF nanopaper. For CNF/GGM films, nanofiber slippage was restricted during deformation due to strong interfacial adhesion between CNF and adsorbed GGM, which resulted in somewhat lower strain to failure. The strong association is efficient also at highly hydrated condition (85 RH %). Hot-pressing resulted in films with improved modulus, which is attributed to better out-of-plane cellulose orientation, favorable CNF–CNF bonding, and reduced porosity. The yield strength at 50 % RH increases due to hot-pressing, which again is related to the same structural factors. The present study shows that GGM may find use as a molecular scale cellulose binding agent causing little sacrifice in mechanical properties at ambient conditions. GGM even shows potential as a wet strength enhancing agent for cellulose materials.

Acknowledgements Financial support from the Wallenberg Wood Science Center (WWSC) and a scholarship fund from the Siam Cement Group (SCG) are gratefully acknowledged. Extraction and analysis of the GGM component are part of the activities at the Johan Gadolin Process Chemistry Center, a Center of Excellence by Åbo Akademi University.

References

1. Sorrentino A, Gorrasi G, Vittoria V (2007) Potential perspectives of bio-nanocomposites for food packaging applications. Trends Food Sci Technol 18:84–95
2. Kisonen V, Prakobna K, Xu C et al (2015) Composite films of nanofibrillated cellulose and O-acetyl galactoglucomannan (GGM) coated with succinic esters of GGM showing potential as barrier material in food packaging. J Mater Sci 50:3189–3199. doi:10.1007/s10853-015-8882-7
3. Carpita NC, McCann MC (2000) Chapter 2 "The cell wall". In: Buchanan BB, Gruissem W, Jones R (eds) Biochemistry and molecular biology of plants. American Society Plant Physiologists, Rockville, pp 52–108
4. Bacic A, Harris PJ, Stone BA (1988) Structure and function of plant cell walls. In: Preiss J (ed) The Biochemistry of Plants. Acedamic Press Inc, New York, pp 297–371
5. Dinwoodie JM (1981) Timber: its nature and behaviour. Van Nostrand Reinhold, New York
6. Xu P, Donaldson LA, Gergely ZR, Staehelin LA (2007) Dual-axis electron tomography: a new approach for investigating the spatial organization of wood cellulose microfibrils. Wood Sci Technol 41:101–116
7. Sakurada I, Nukushina Y, Ito T (1962) Experimental determination of the elastic modulus of crystalline regions in oriented polymers. J Polym Sci 57:651–659
8. Sturcova A, Davies GR, Eicchorn S (2006) Elastic modulus and stress-transfer properties of tunicate cellulose whiskers. Biomacromolecules 6:1055–1061
9. Iwamoto S, Kai W, Isogai A, Iwata T (2009) Elastic modulus of single cellulose microfibrils from tunicate measured by atomic force microscopy. Biomacromolecules 10:2571–2576
10. Saito T, Kuramae R, Wohlert J, Berglund LA, Isogai A (2013) An ultrastrong nanofibrillar biomaterial: the strength of single cellulose nanofibrils revealed via sonication-induced fragmentation. Biomacromolecules 14:248–253
11. Henriksson M, Henriksson G, Berglund LA, Lindström T (2007) An environmentally friendly method for enzyme-assisted preparation of microfibrillated cellulose (MFC) nanofibers. Eur Polym J 43:3434–3441
12. Saito T, Nishiyama Y, Putaux JL, Vignon M, Isogai A (2006) Homogeneous suspensions of individualized microfibrils from TEMPO-catalyzed oxidation of native cellulose. Biomacromolecules 7:1687–1691
13. Turbak AF, Snyder FW, Sandberg KR (1983) Microfibrillated cellulose, a new cellulose product: properties, uses, and commercial potential. J Appl Polym Sci 37:815–827
14. Hansen NML, Blomfeldt TOJ, Hedenqvist MS, Plackett DV (2012) Properties of plasticized composite films prepared from nanofibrillated cellulose and birch wood xylan. Cellulose 19:2015–2031
15. Mikkonen KS, Stevanic JS, Joly C et al (2011) Composite films from spruce galactoglucomannans with microfibrillated spruce wood cellulose. Cellulose 18:713–726
16. Stevanic JS, Mikkonen KS, Xu C, Tenkanen M, Berglund L, Salmen L (2015) Wood cell wall mimicking for composite films of spruce nanofibrillated cellulose with spruce galactoglucomannan and arabinoglucuronoxylan. J Mater Sci 49:5043–5055. doi:10.1007/s10853-014-8210-7
17. Prakobna K, Terenzi C, Zhou Q, Furo I, Berglund LA (2015) Core-shell cellulose nanofibers for biocomposites—nanostructural effects in hydrated state. Carbohydr Polym 125:92–102
18. Sjöström E (1993) Wood chemistry: fundamentals and applications. Academic Press Inc., San Diego, pp 51–70
19. Willför S, Sjöholm R, Laine C, Roslund M, Hemming J, Holmbom B (2003) Characterisation of water-soluble galactoglucomannans from Norway spruce wood and thermomechanical pulp. Cabohydr Polym 52:175–187
20. Willför S, Sundberg A, Hemming J, Holmbom B (2005) Polysaccharides in some industrially important softwood species. Wood Sci Technol 39:245–257
21. Hartman J, Albertsson AC, Lindblad MS, Sjöberg J (2006) Oxygen barrier materials from renewable sources: material properties of softwood hemicellulose-based films. J Appl Polym Sci 100:2985–2991

22. Mikkonen KS, Heikkilä MI, Helen H, Hyvönen L, Tenkanen M (2010) Spruce galactoglucomannan films show promising barrier properties. Carbohydr Polym 79:1107–1112
23. Mikkonen KS, Yadav MP, Cooke P, Willför S, Hicks KB, Tenkanen M (2008) Films from spruce galactogluccomannan blended with poly(vinyl alcohol), corn arabonoxylan, and konjac glucomannan. Bioresource 3:178–191
24. Teeri TT, Brumer H, Daniel G, Gatenholm P (2007) Biomimetic engineering of cellulose-based materials. Trends Biotechnol 25:299–306
25. Svagan AJ, Azizi Samir MAS, Berglund LA (2007) Biomimetic polysaccharide nanocomposites of high cellulose content and high toughness. Biomacromolecules 8:2556–2563
26. Olszewska A, Valle-Delgado JJ, Nikinmaa M, Laine J, Österberg M (2013) Direct measurements of non-ionic attraction and nanoscaled lubrication in biomimetic composites from nanofibrillated cellulose and modified carboxymethylated cellulose. Nanoscale 5:11837–11844
27. Prakobna K, Galland S, Berglund LA (2015) High-performance and moisture-stable cellulose-starch nanocomposites based on bioinspired core-shell nanofibers. Biomacromolecules 16: 904–912
28. Henriksson M, Berglund LA, Isaksson P, Lindström T, Nishino T (2008) Cellulose nanopaper structure of high toughness. Biomacromolecules 9:1579–1585
29. Sehaqui H, Zhou Q, Berglund LA (2011) Nanostructured biocomposites of high toughness—a wood cellulose nanofiber network in ductile hydroxyethylcellulose matrix. Soft Matter 7:7342–7350
30. Lucenius J, Parikka K, Österberg M (2014) Nanocomposite films based on cellulose nanofibrils and water-soluble polysaccharides. React Funct Polym 85:167–174
31. Whitney SEC, Gothard MGE, Mitchell JT, Gidley MJ (1999) Roles of cellulose and xyloglucan in determining the mechnaical properties of primary plant cell walls. Plant Physiol 121:657–663
32. Chanliaud E, Burrows KM, Jeronimidis G, Gidley MJ (2002) Mechanical properties of primary plant cell wall analogues. Planta 215:989–996
33. Cybulska J, Vanstreels E, Ho QT et al (2010) Mechanical characteristics of artificial cell walls. J Food Eng 96:287–294
34. Willför S, Rehn P, Sundberg A, Sundberg K, Holmbom B (2003) Recovery of water-soluble acetylgalactoglucomannans from mechanical pulp of spruce. Tappi J 2:27–32
35. Xu C, Eckerman C, Smeds A, Reunanen M, Eklund PC, Sjöholm R, Willför S (2009) Rheological properties of water-soluble spruce O-acetyl galactoglucomannans. Carbohydr Polym 75:p498–p504
36. Michielsen S (1999) Specific refractive index increments of polymers in dilute solution. In: Brandrup J, Immergut EH, Grulke EA (eds) Polymer handbook. Wiley, New York pp, pp 547–627
37. Sundberg A, Kenneth S, Lillandt C, Holmbom B (1996) Determination of hemicelluloses and pectins in wood and pulp fibres by acid methanolysis and gas chromatography. Nord Pulp Paper Res J 11:216–219
38. Sehaqui H, Liu A, Zhou Q, Berglund LA (2010) Fast preparation procedure for large, flat cellulose and cellulose-inorganic nanopaper structures. Biomacromolecules 11:2195–2198
39. Sehaqui H, Zhou Q, Ikkala O, Berglund LA (2011) Strong and tough cellulose nanopaper with high specific surface area and porosity. Biomacromolecules 12:3638–3644
40. Whitney SEC, Brigham JE, Darke AH, Reid JSG, Gidley MJ (1998) Structural aspects of the interaction of mannan-based polysaccharides with bacterial cellulose. Cabohydr Res 307:299–309
41. Eronen P, Österberg M, Heikkinen S, Tenkanen S, Laine J (2011) Interactions of structurally different hemicelluloses with nanofibrillar cellulose. Carbohydr Polym 86:1281–1290
42. Vincken JP, Keizer AD, Beldman G, Voragen AGJ (1995) Fractionation of xyloglucan fragments and their interaction with cellulose. Plant Physiol 108:1579–1585
43. Xu C, Eckerman C, Smeds A et al (2011) Carboxymethylated spruce galactoglucomannans: preparation, characterisation, dispersion stability, water-in-oil emulsion stability, and sorption on cellulose surface. Nord Pulp Paper Res J 26:167–178
44. Hubbe MA, Rojas OJ (2008) Colloidal stability and aggregation of lignocellulosic material in aqueous: a review. BioResources 3:1419–1491
45. Fall AB, Lindström SB, Sundman O, Ödberg L, Wågberg L (2011) Colloidal stability of aqueous nanofibrillated cellulose dispersions. Langmuir 27:11332–11338
46. Fernandes AN, Thomas L, Altaner CM et al (2011) Nanostructure of cellulose microfibrils in spruce wood. PNAS Plus 108:E1195–E1203
47. Whitney SEC, Brigham JE, Darke AH, Reid JSG, Gidley MJ (1995) In vitro assembly of cellulose/XG networks: ultrastructure and molecular. Plant J 8:491–504
48. Nilsson H, Galland S, Larsson PT, Gamstedt EK, Nishino T, Berglund LA, Iversen T (2010) A non-solvent approach for high-stiffness all-cellulose biocomposites based on pure wood cellulose. Compos Sci Technol 70:1704–1712
49. Nilsson H, Galland S, Larsson PT, Gamstedt EK, Iversen T (2012) Compression molded wood pulp biocomposites: a study of hemicellulose influence on cellulose supramolecular structure and material properties. Cellulose 19:751–760
50. Salmen L, Olsson AM (1998) Interaction between hemicelluloses, lignin and cellulose: structure and property relationships. J Pulp Pap Sci 24:99–103
51. Kelly A (1970) Interface effects and the work of fracture of a fibrous composite. Proc R Soc Lond A 319:95–116
52. Brunauer S (1943) The adsorption of gases and vapors-I physical adsorption. Princeton University Press, Princeton
53. Obataya E, Norimoto M, Gril J (1998) The effects of adsorbed water on dynamic mechanical properties of wood. Polymer 39:3059–3064
54. Luo HL, Lian JJ, Wan YZ, Huang Y, Wang YL, Jiang HJ (2006) Moisture absorption in VARTMed three-dimensional braided carbon-epoxy composites with different interface conditons. Mater Sci Eng A 425:70–77